2016

Noninvasive Measurement of Electrical Events Associated with a Single Chlorovirus Infection of a Microalgal Cell

Seung-Woo Lee
University of Nebraska–Lincoln

Eun-Hee Lee
University of Nebraska–Lincoln

Gerhard Thiel
Technische Universität Darmstadt, Germany, thiel@bio.tu-darmstadt.de

James L. Van Etten
University of Nebraska-Lincoln, jvanetten1@unl.edu

Ravi Saraf
University of Nebraska-Lincoln, rsaraf2@unl.edu

Noninvasive Measurement of Electrical Events Associated with a Single Chlorovirus Infection of a Microalgal Cell

Seung-Woo Lee,[1,4] Eun-Hee Lee,[1,5] Gerhard Thiel,[2] James L. Van Etten,[3] and Ravi F. Saraf[1,6]

1 Department of Chemical and Biomolecular Engineering, University of Nebraska–Lincoln, Lincoln, Nebraska 68588, United States
2 Department of Biology, Technische Universität-Darmstadt, Schnittspahnstrasse 3, Darmstadt 64287, Germany
3 Department of Plant Pathology and Nebraska Center for Virology, University of Nebraska–Lincoln, Lincoln, Nebraska 68583, United States
4 Post-Silicon Semiconductor Institute, Korea Institute of Science and Technology (KIST), Hwarang-ro 14-gil 5, Seongbuk-gu, Seoul 02792, Republic of Korea
5 Department of Environmental Science and Engineering, Ewha Womans University, Ewhayeodae-gil 52, Seodaemun-gu, Seoul 03760, Republic of Korea
6 Nebraska Center for Materials and Nanosciences, University of Nebraska–Lincoln, Lincoln, Nebraska 68588, United States

Authors S.-W. Lee and E.-H. Lee contributed equally to this paper.

Corresponding author — R. Saraf, email rsaraf2@unl.edu

Abstract

Chlorovirus *Paramecium bursaria* chlorella virus 1 (PBCV-1) contains a viral-encoded K^+ channel imbedded in its internal membrane, which triggers host plasma membrane depolarization during virus infection. This early stage of infection was monitored at high resolution by recording the cell membrane depolarization of a single *Chlorella* cell during infection by a single PBCV-1 particle. The measurement was achieved by depositing the cells onto a network of one-dimensional necklaces of Au nanoparticles, which spanned two electrodes 70 μm apart. The nanoparticle necklace array has been shown to behave as a single-electron device at room temperature. The resulting

Published in *ACS Nano* 10 (2016), pp 5123–5130.
DOI: 10.1021/acsnano.6b00299

Submitted January 14, 2016; accepted May 3, 2016; published May 3, 2016.
Supporting Information follows the References.

electrochemical field-effect transistor (eFET) was gated by the cell membrane potential, which allowed a quantitative measurement of the electrophysiological changes across the rigid cell wall of the microalgae due to a single viral attack at high sensitivity. The single viral infection signature was quantitatively confirmed by coupling the eFET measurement with a method in which a single viral particle was delivered for infection by a scanning probe microscope cantilever.

Keywords: field-effect transistor, viral infection, cell membrane potential, depolarization, electrochemical analysis

Since the discovery that the M2 protein from influenza virus A has ion-channel activity,[1] other ion-channel forming viral proteins, such as BM2 and NB by influenza virus B, CM2 by influenza virus C, and Vpr and Vpu by HIV-1, have been discovered.[2] Analogous to ion channels in cellular membranes, these proteins, called viroporins, enhance the conductance in membranes of host cells.[2] Viroporins like M2 in influenza virus A, P7 from hepatitis virus C, or Vpu from HIV-1 are inserted into the plasma membrane of the host and eventually cause a dissipation of the host membrane potential.[2] Viroporins, which facilitate the transport of ions and small molecules during various stages of infection, are also found in viruses, which infect the unicellular green microalga *Chlorella*. These chloroviruses use a viral-encoded K^+ channel during infection of their

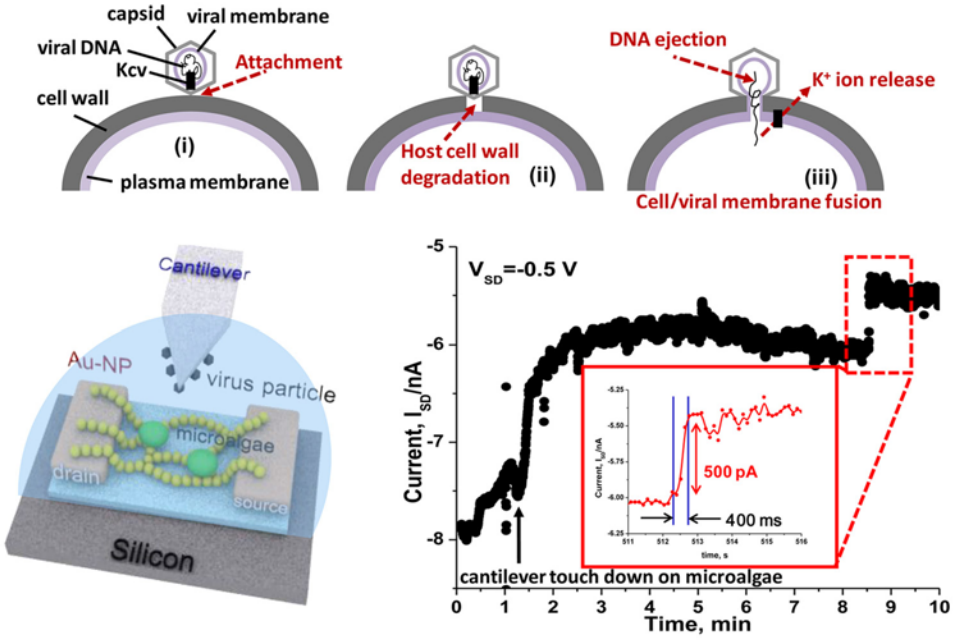

single-celled algal hosts.[3] While the precise function of many viroporins is still unknown, it is well established that the activity of others is essential at different stages of viral infection.[2] A viroporin generated depolarization of the host membrane enhances the release of many enveloped viruses like HIV-1.[4] In the case of some bacteriophages and in chloroviruses, the viroporin triggered depolarization is essential for the initial infection of the host cells.[3,5] Hence, understanding viroporin function and inhibiting viroporin activity is being explored as a potential antiviral strategy.[6] Thus, the development of noninvasive, electrophysiological methods could be used to monitor the kinetics of the infection process or the release of viral progeny and to study the efficacy of antiviral drugs.

Typically, the electrical properties of cells are studied either electronically or optically. While electronic methods directly quantify membrane potential modulations in an invasive manner, the optical procedure has the advantage of being noninvasive. Optical methods, using voltage-sensitive dyes, can visualize membrane potential modulations only in an indirect manner by monitoring fluorescence changes.[7] It is, therefore, difficult to use these dyes to quantify membrane potential modulation in a single virus attack involving the activity of only one or more ion channels. Arguably, the most sensitive electrometer to measure potential modulation is the transistor because almost no current flows from the entity measured (*i.e.*, the cell) into the device (*i.e.*, the transistor). Therefore, an electrochemical field-effect transistor (eFET) can noninvasively measure membrane potential modulation in a cell.[8−10] The (membrane) potential modulation of a cell deposited on an eFET changes the local charge (distribution) at the device/cell interface, causing the current to change, *i.e.*, gating. As a result, the sensitivity of the transistor depends on how sensitive the device current is to the local charging. The smaller the transistor, the greater the sensitivity to charge.[11,12] Recently, with the use of nanoparticles, the smallest possible structural unit, a single-electron eFET, was described[13] with a gain that was ∼3-fold higher than that of Si nanowire,[14] ∼5-fold higher than that of carbon nanotubes,[15] and 2.5-fold larger than that of graphene-based eFETs.[16] The high sensitivity of the nanoparticle-based eFET allowed a quantitative measurement of a change in cell membrane potential during photosynthesis in a green microalga caused by a light-induced proton gradient in the thylakoid membrane inside the cell.[17]

Results and discussion

The structure, fabrication, and mechanism of nanoparticle-based eFET[17] and corresponding biogating were previously described in the literature.[13] Briefly, the nanoparticle eFET is a monolayer array of 10 nm Au nanoparticles forming a network of 1D necklaces between two Au electrode pads spanning a distance of 70 μm (Figure 1a, inset 1). The thickness of the electrodes was 50 nm to ensure strong interconnection across the step. The darker region in the SEM image, *i.e.*, circuitry and part of the electrode, was due to the photoresist, SU8 coating, during photolithography. The network array was fabricated in a two-step process (see Methods, Section 1). In the first step, a 1D single file of necklaces of negatively charged 10 nm Au nanoparticles was obtained in solution by directed self-assembly of uniformly charged spherical (non-Janus) particles mediated by multivalent cations. In the second step, the necklaces were deposited in a well-defined array between the source and the drain electrode on a 210 μm wide PDMS strip printed by soft lithography (Figure 1a, inset 2). To illustrate the quality of printing, the PDMS lines in the optical image are 10-fold narrower (*i.e.*, 20 μm) than those used for ion-channel studies.

The array in air at room temperature exhibited a strong Coulomb blockade where the current, I, across the array as a function of applied bias, V, between the source and the drain, showed a threshold bias, V_T (Figure 1b). The large V_T was due to a cumulative Coulomb blockade from single-electron charging on multiple nanoparticles along the percolation path, called the random quenched charge disorder (rQCD) (schematically shown in Figure 1b, inset as charge centers). The single-electron charge was trapped in randomly located, isolated particles in the percolation path where the tunneling resistance between the adjacent particles was larger than $\sim h/e^2$ (where e and h are charge on an electron and Planck's constant, respectively). The result of this single-electron charging in the rQCD, as observed in Figure 1b, was a scaling behavior where $I \sim (V - V_T)^{\zeta}$, and ζ was a scaling exponent of ~2.[18] Conventionally, the single-electron effect is observed at cryogenic temperatures in a nanoparticle array with a source-drain gap of below 5 μm.[18] The remarkably robust single-electron effect at room temperature, corresponding to a blockade energy of ~2.1 eV (*i.e.*, $\sim 80kT$, where k is the Boltzmann constant and T is the device temperature) over a gap in the 70 μm range, was attributed to the local 1D necklace structure.[18–20]

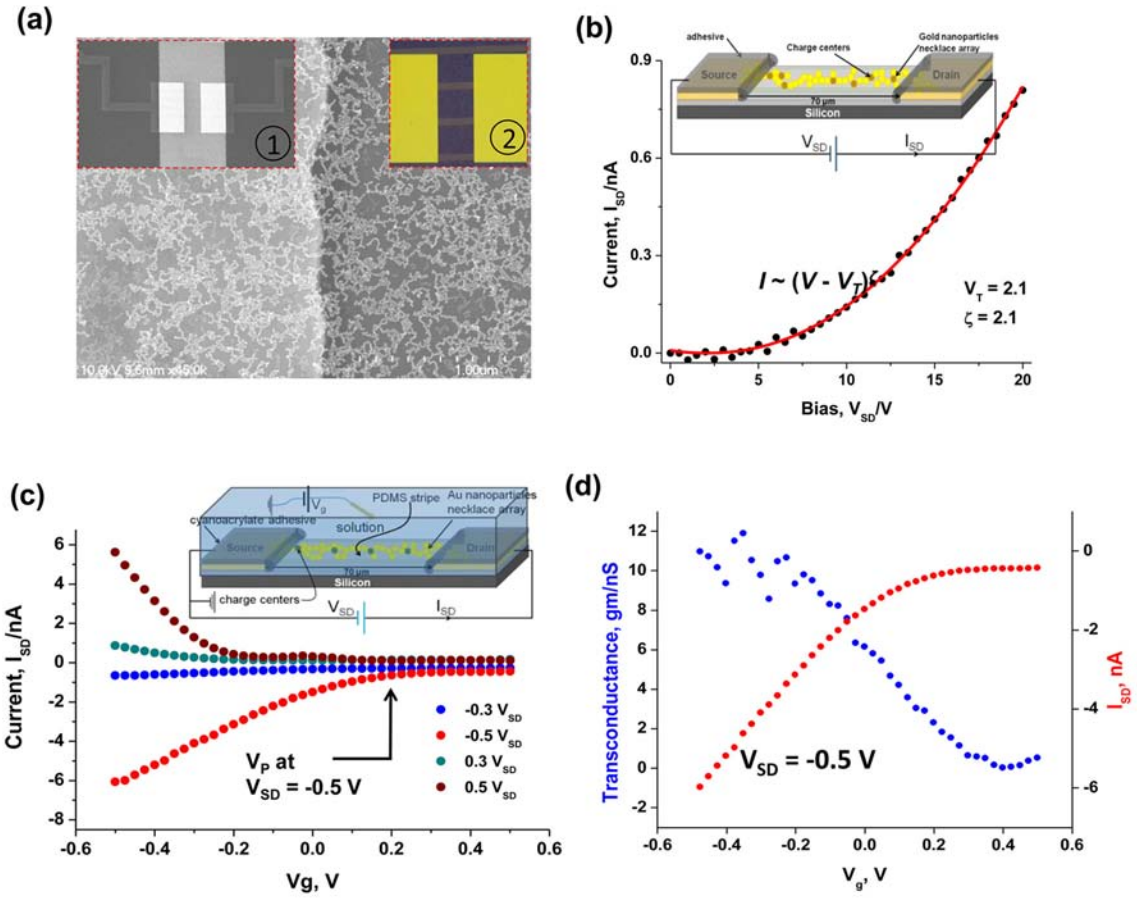

Figure 1. Characterization of a single-electron eFET device. **(a)** Scanning electron microscope (SEM) image of the Au NP necklace network device. Inset 1: SEM image of the Au electrodes. The darker region in the SEM image shows passivation of the electrodes with photoresist via photolithography. Inset 2: optical microscope image of PDMS strips printed on the source and drain electrodes. **(b)** I–V characteristics of the single-electron eFET device in air and the fitting curve to experimental data for the estimation of V_T and ξ values. Inset: schematic of the single-electron eFET device. **(c)** Electrochemical gating behavior of the nanoparticle necklace array in aqueous solution. I_{SD} vs V_g behavior as a function of a fixed V_{SD}, showing the gating nature of the device. The arrows indicate the pinch-off voltage (V_p) at the given V_{SD}. V_g is applied by the Ag/AgCl reference electrode. Inset: schematic of experimental setup for the electrochemical gating assay. **(d)** Transconductance behavior of the necklace array without microalgae at a fixed V_{SD} of −0.5 V.

The mechanism of gating modulates the distribution of rQCD to alter the landscape of the energy barrier height due to local single-electron charging.[13,17] Similar to conventional eFET characterization, the necklace was immersed in electrolyte solution, and the source and drain

electrodes were hermetically sealed with an adhesive (see Methods, Section 1). A potential, V_{SD}, was applied between the source and drain electrodes, and the current, I_{SD}, was measured (see Methods, Section 2). To gate I_{SD}, the potential between the solution and the source electrode, V_g, was applied using a standard Ag/AgCl reference electrode (Figure 1c, inset).[13] It is important to note that because the reference electrode had very large impedance, no current flowed from it to the device. The reference electrode was a true gating electrode. At a fixed V_{SD}, as V_g was regulated, the device current, I_{SD}, changed, exhibiting typical eFET gating behavior (Figure 1c). The I_{SD} was completely blocked for V_g higher than a certain bias, V_p, called the pinch-off potential, as reported earlier.[13]

The sensitivity and quantification of the membrane potential depends on the transconductance, g_m, of the eFET (Figure 1d). For eFET, $g_m = (dI_{SD}/dV_g)$ at fixed V_{SD} is the relative sensitivity of the device, *i.e.*, the larger the g_m at a given V_{SD}, the higher the response, *i.e.*, change in I_{SD}, for a given stimulation, *i.e.*, change in V_g. For the necklace array eFET, the sensitivity was largest when $V_g < 0$. As the cell's resting membrane potential was near 0 V, the sensitivity of the device for our interest was about 8 nS. As the cells did not occupy the whole device and infection was localized to a single cell, the relationship between membrane potential change and I_{SD} was modified (as will be discussed later with respect to the model in Supporting Information, Sections D–F). As the electrophysiology studies were performed at $V_g = 0$ mV (to avoid electrical perturbation in the cell) and the resting potential of the membrane was about −100 mV, a V_{SD} of −0.5 V was an optimum condition for electrophysiology measurement. The larger the channel length, L, the more enhanced was the single-electron gating effect due to more incidences of charge centers. This is in contrast to nanowire and graphene, where $g_m \sim 1/L$ and $1/L^2$, respectively.[11,12] Thus, a larger eFET with more cells to capture a single viral infection at higher probability is possible. An L of 70 nm was chosen because above 100 nm, the resistance becomes too large for a stable signal.

In the study described here, the large (190 nm), icosahedral, plaque-forming, dsDNA (330 kb), chlorovirus PBCV-1[21] was chosen to study well established early electrical events during a single infection of its host, *Chlorella variabilis* (see details in Methods, Section 3) using the nanoparticle-based eFET system described above. The PBCV-1 virion has an internal lipid bilayered membrane surrounded by an outer glycoprotein

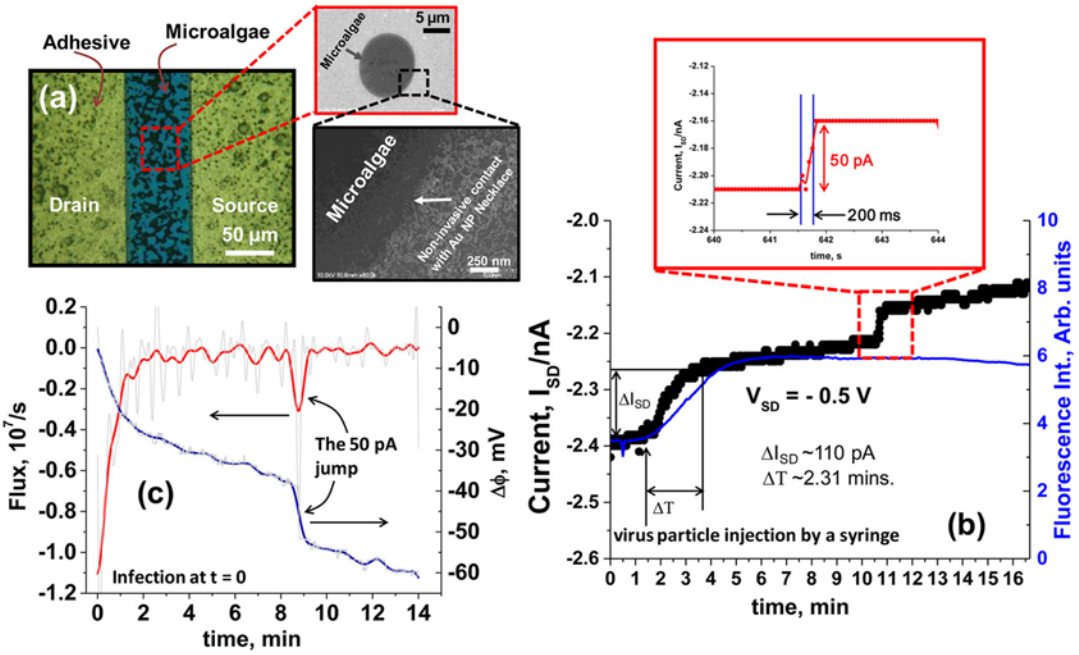

Figure 2. Noninvasive measurement of viral infection of a microalga using an eFET device. **(a)** Optical microscope image of the device where C. variabilis cells were deposited between the hermetically sealed Au electrodes. Top inset: SEM image of the microalga deposited on the Au NP necklace array. Bottom inset: SEM image of the microalga, which has noninvasive contact with Au NP necklace arrays. **(b)** Current changes measured by the eFET device during viral infection following addition of viral particles by syringe injection. The ΔT (and corresponding ΔI) are the initial rapid rise of the response before the signal nominally plateaus. The blue line is a virus-triggered membrane depolarization curve that was monitored with the voltage-sensitive fluorescent dye bisoxonol. The lower rise of the fluorescence curve was qualitatively aligned with the injection point of eFET data to guide the comparison. Inset: magnification of an instantaneous current jump. V_{SD} and V_g were fixed at −0.5 V and 0 mV, respectively. **(c)** The K^+-flux and membrane potential as a function of time corresponding to the measured ΔI_{SD} response in (b). The Δφ was set to zero at the time of infection (t = 0). The light gray lines are raw data before smoothing.

capsid. During infection, the PBCV-1 membrane, which contains a viral-encoded K^+ channel called Kcv, fuses with the host plasma membrane[22] which triggers rapid depolarization of the host cell membrane and subsequent K^+ efflux from the cell (see Supporting Information, Section B and Figure S2).[3]

To study cell membrane potential modulation during a virus attack, *C. variabilis* cells were deposited on a necklace array device. Consistent with previous studies on real-time photosynthesis[17] and cell

metabolism,[23] the microalgae adhered to the necklace array forming good electrical contact (Figure 2a). The good adhesion and electrical contact between the cell and the necklace array is attributed to the nanostructured nature of the Au nanoparticle-based device, as reported for eFET studies on the effect of structural roughness dimension on cell-membrane-influenced gating.[24] About 10^7 chlorovirus particles were injected into the chamber containing the eFET device in contact with MBBM medium with 0.5 mM $MgCl_2$ and 2.7 mM KCl (see details Section 4 in Methods and Figure S3 in Supporting Information). The device bias, V_{SD} = −0.5 V and V_g = 0 mV, was applied, and the change in current, I_{SD}, was monitored (Figure 2b).

At a fixed V_{SD}, the I_{SD} was stable at about −2.4 nA (Figure 2b). As the injected virus solution approached the device (∼2 min in Figure 2b), a rapid increase was recorded. Due to the small solid angle subtended by the device and low probability of cell–virus binding that occurs at a unique viral vertex,[25] presumably only one infection was recorded by the device. In about 50% of the experiments, no infection occurred (Supporting Information, Section C, Figure S4). The response with no viral infection was similar to the control where the injected solution was of the same buffer composition but had no virus (Figure 3a), *i.e.*, the control. The second control (Figure 3b) is discussed later in context with Figure 4. The response of the control and no viral infection is flat with a stable current, except for a small perturbation at the injection due to fluid flow that presumably perturbs the EDL. The current change for the control and no-infection responses was significantly smaller than the response with a viral infection (Figure 2b), as signified by plotting the graphs with a similar range for I_{SD}. The baseline currents for all three responses are slightly different due to variations in the necklace array deposition. The assumption that the response curve corresponded to a single infection was independently supported using a scanning probe microscope (SPM) cantilever (see below, Figure 4).

The initial response was consistent with the early events associated with PBCV-1 infection (Supporting Information, Figure S2). More importantly, the eFET response curve resembled the virus-triggered membrane depolarization curve that was monitored with the voltage-sensitive fluorescent dye, bisoxonol (Figure 2b). Membrane depolarization resulted in K^+ release from the microalga.[3] However, the fluorescent dye is known to exhibit a slow response and a nonlinear dependency on

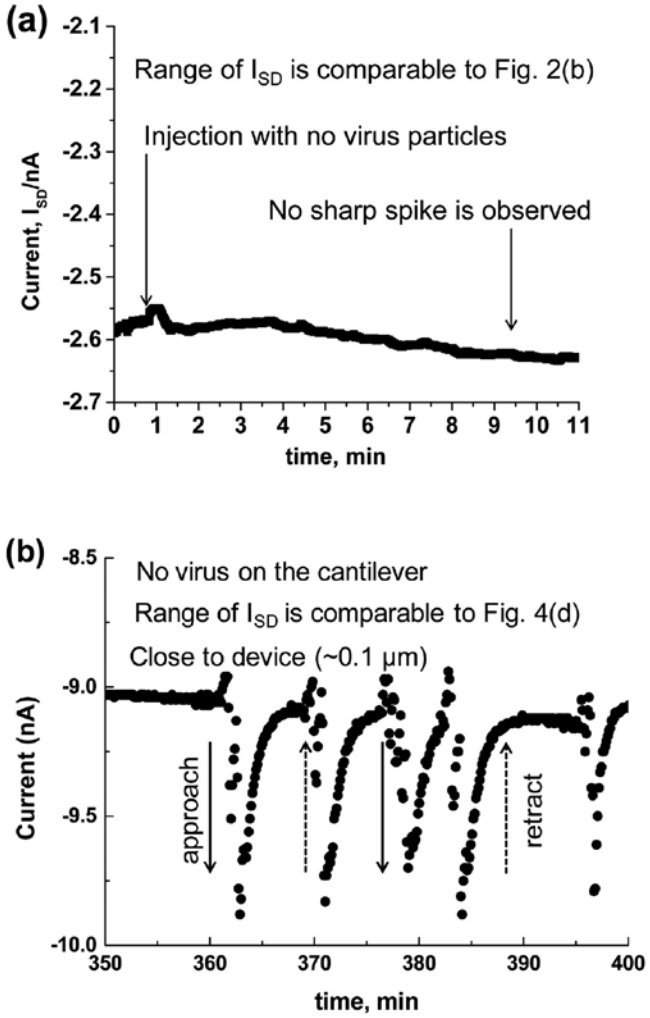

Figure 3. Response of the eFET necklace array on exposure to an external stimulus with no virus particles (controls). **(a)** Device response due to injection of buffer fluid with no virus particles. The composition of the buffer solution injected was the same as that shown in Figure 2b. **(b)** Device response to "blank" cantilever with the same surface modification as in Figure 4d except there was no virus deposition.

rapid changes in the membrane voltage.[7] Therefore, the fluorescent signal was indeed predicted to slightly lag behind the electrical signal (Figure 2b). The sharper "rise" in I_{SD} than in the fluorescence response was also due to the fact that the eFET signal monitored a single infection, in contrast to the fluorescence study which is an average of many cells. However, the overall similarity of the two signals strongly supports the inference that the eFET response was due to a virus-induced change in membrane voltage.

To quantify the temporal nature of the response, a simple model was developed to estimate the change in the membrane potential, $\Delta\varphi$, due to infection with respect to the cell's resting membrane potential, φ_M (at $t = 0$ before infection) as well as a calculation of the K^+ ion-flux from the cell (see details in Supporting Information, Sections D–F). For *Chlorella*, $\varphi_M \approx -125$ mV.[26] From the model (Supporting Information, Section D), the change membrane potential, $\Delta\varphi$, can be calculated from change in current, ΔI_{SD} as

$$\Delta\varphi = \varphi - \varphi_M = -\left[\frac{1}{(7f-1)}\left(1+\left\{\frac{g_{m,S}}{g_{m,C}}\right\}\frac{f}{1-f}\right)^{-1}+1\right]$$

$$\frac{1}{g_{m,C}}\Delta I_{SD} = -k\frac{1}{g_{m,C}}\Delta I_{SD} \quad (1)$$

where f is the area coverage of the cell on the network, and $g_{m,S}$ and $g_{m,C}$ are the transconductance of the network exposed to the solution and under the cell, respectively (Supporting Information, Figure S5). Of note is that $\neq g_{m,C}$ because they are at different gating potentials, as discussed below. For the rapid rise in $\Delta I_{SD} = 110$ pA (Figure 2b), from Eq. 1, the $\Delta\varphi$ is ~28 mV. The local effective transconductance for the network under the infected cell, $g_{m,C} = \Delta I_{SD}/\Delta\varphi \approx 7.9$ nS, which was consistent with $g_{m,C} \sim 8$ nS for $\varphi_M \approx -125$ mV (Figure 1d and Section E in Supporting Information). The consistency in $g_{m,C}$ indicated that the charge centers were uniformly distributed, leading to constant transconductance ($g_{m,C}$ or $g_{m,S}$) over the array. The quantitative change in the membrane potential based on Eq. 1 (with details in Supporting Information, Section E), is shown in Figure 2c. The details of the ion-flux calculations are shown in Supporting Information, Section F (Eqs. (8)–(10)). Briefly, from $\Delta I_{SD}(t)$ response in Figure 2b, $\Delta\varphi(t)$ is calculated using Eq. 1 which is substituted in Supporting Information, Eq. (9) (*i.e.*, Nernst Equation) to calculate ion concentration as a function of time, *t*. Subsequently, taking the derivative of the ion concentration (Supporting Information, Eq. (10)) the flux is calculated. The value of $dN/dt \sim 10^7$ ions/s was reasonable considering that even a single channel with a large conductance like Kcv[27] can transport this number of ions. The flux response indicated that most of the ion-mediated infection process was completed within 2 min (Figure 2c). The early rise at 2 min agrees with the time the virus takes to attach to the *Chlorella* cell and degrade the cell wall at the point

of attachment, which then allows the virus membrane to fuse with the host plasma membrane and ultimately leads to depolarization and release of K^+ into the medium.[23,28]

In addition to the early virus-triggered depolarization, a rapid decrease in the eFET signal routinely occurred ~8 min postinfection (Figure 2b,c). Compared to the control (Figure 3a), and no-viral-infection samples (Supporting Information, Figure S4), the sudden jump at ~8 min occurred only on successful viral infection, suggesting that the two increases were causally related (discussed below). This jump response did not appear in the fluorescence recording.

To confirm that the eFET signal was caused by a single infection event, we developed a method to obtain "viral infection on demand". Negatively charged PBCV-1 particles were placed on a 50 μm wide cantilever coated with positively charged poly(L-lysine) (PLL) (see details in Methods, Section 5) at sparse coverage of ~2 particle/100 μm^2 (Figure 4a,b). The tip of the cantilever was brought into contact with the *Chlorella* cell using a motorized nanopositioner. Touchdown was monitored by a change in the reflected light due to slight bending of the cantilever (Figure 4c). The cantilever was not moved during the recording to avoid complications from environmental changes during the infection process. The I_{SD} response of the eFET in Figure 4d resembled the response in Figure 2b, *i.e.*, a relatively slower increase in current followed by a jump. Owing to the icosahedron shape of the virus and only a few specific binding sites to the cell, no infection occurred on touchdown in ~50% of instances (see Supporting Information, Figure S4b). Similar to the injection case (Supporting Information, Figure S4a), the I_{SD} was reasonably unchanged for no infection (Supporting Information, Figure S4b) compared to the response upon viral infection (Figure 4d). The low incidence of infection with sparse coverage of particles on the cantilever indicates that the response was from a single viral infection. The biphasic signal shown in both Figure 2b and Figure 4d suggests that the single jump was a signature of a single viral infection event. Multiple jumps were never observed, indicating only one viral infection.

There were two important differences in the results between the injection and the cantilever experiments: (i) the response time was significantly faster in the cantilever experiment, *i.e.*, ΔT was 7-fold faster; and (ii) the modulation in membrane potential was larger. The larger magnitude in ΔI_{SD} was expected due to gating from the cantilever. The

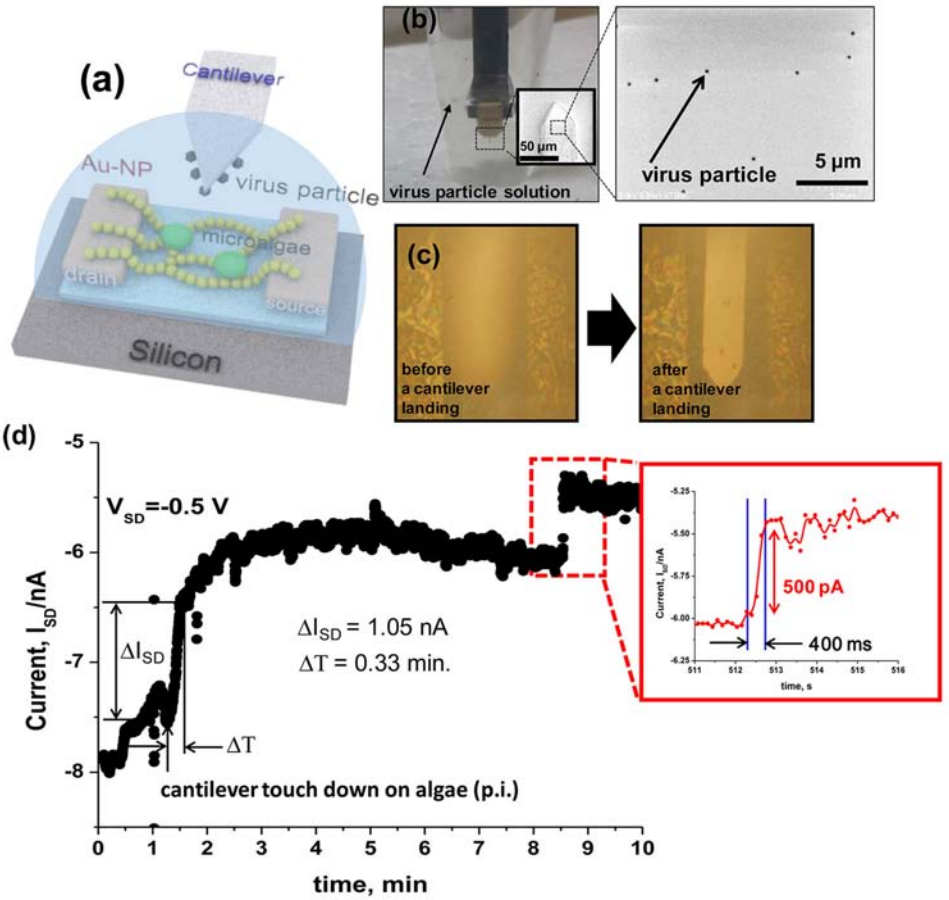

Figure 4. Biogating response caused by the viral infection of an microalga that was introduced by a scanning probe microscope cantilever system. **(a)** Schematic of the direct delivery of virus particles on microalgae by using a scanning probe microscope cantilever. **(b)** Optical image of the scanning probe microscope cantilever, which was immersed in a virus solution. Inset: SEM images of the virus particles that were immobilized on the surface of the cantilever. **(c)** Optical microscope images of the cantilever before and after landing between the source and drain electrodes. **(d)** Current changes measured by the eFET device during the viral infection process of the microalga using the cantilever infection method. Similar to Figure 2b, the ΔT (and the corresponding ΔI) was defined by the high change region before the rate began to decrease. Inset: magnification of the instantaneous current jump. V_{SD} and V_g were fixed at −0.5 V and 0 mV, respectively.

potential of zero charge (PZC) of the cantilever coated with a positively charged polyelectrolyte was about −300 mV.[17] As a result, the proximity of the cantilever (due to the electrical double layer with negatively charged ions) effectively gated the necklace array to produce a larger conductance, g_m of ~11 nS at V_g of ~ −300 mV (Figure 1d). The control

experiment with no viral particles was consistent with the cantilever-influenced gating (Figure 3b). Initially, the cantilever (~50 μm wide), at a distance of ~100 nm, partially gated the device leading to a baseline current of ~9 nA. As the cantilever was moved (approached or retracted) at a speed of 200 nm/min, the vibration of the cantilever spread the negative ions from the region below the cantilever over the rest of the device. The effective g_m dropped, leading to an increase in (negative) current. When the perturbed EDL over the uncovered device relaxed, the current was restored. This indicates that the current due to the cantilever approach was reasonably stable except during the vibration caused by the motion.

The 3-fold increase (before infection) in I_{SD} (comparing the base current of about −2.4 and −7.5 nA in Figures 2b and 4d, respectively) was significantly larger than the expected conductivity increase from transconductance (from 6 to 11 nS in Figure 1d). The discrepancy may be attributed to the physical interaction between the cell and cantilever, such as squeezing, as indicated below. From Eq. 1, for $f = 0.15$ and $\Delta I_{SD} = 1.05$ nA, $\Delta\varphi$ is ~140 mV, a 10-fold increase compared to diffusion-mediated infection (Figure 2b). Similar to calculations for Figure 2b, for consistency, the local effective transconductance for the network under the infected cell was $g_m = \Delta I_{SD}/\Delta\varphi \approx 7.6$ nS, which agreed with $g_m \sim 8$ nS at $V_g = \varphi_M = -125$ mV for the array (Figure 1d).

There are several explanations for why the cantilever delivery of the virus enhanced the effects of infection. A rate-limiting step in the initial infection process was the time required to degrade the cell wall. It is likely that "squeezing" the virus against the host cell favored local activity of the wall-digesting enzyme(s) since it reduced diffusion from the site of action. An additional rate-limiting step could be the fusion between the viral and host membranes. It has been proposed that pressure is required for fusion of the two membranes.[3] Therefore, "squeezing" the cell with the virus-coated cantilever probably enhanced membrane fusion. Next, we considered the rapid change in I_{SD} at a subsecond scale curve 7−9 min after infection (Figures 2b and 4d). Since this late jump in the eFET signal was not observed in the fluorescence measurements (Figure 2b), it is unlikely it was caused by a direct electrical event. A plausible explanation for the late signal is a biomechanical effect. We suspect that partial detachment between the infected cell and the nanoparticle necklace network occurs during infection. There are two possible explanations for partial detachment: (i) cell plasmolysis that caused

detachment of the plasma membrane from the cell wall[3] and/or (ii) the cell moved because of the momentum from the DNA injection. As the jump in current observed in Figure 2c at ~8 min is due to biomechanical reason, the corresponding effective membrane potential jump and the ion-flux peak are simply an artifact of the calculations (*i.e.*, in Supporting Information, Eqs. (7)–(10)).

Conclusions

We demonstrated that a nanoparticle necklace array eFET has the sensitivity to quantitatively measure, in a noninvasive manner, the impact of viral ion channels on the conductance of an individual host cell in real time. Ion channel activity was induced during virus PBCV-1 infection of its host *Chlorella* cell. An interesting aspect of eFET is its ability to measure membrane potential modulation in an microalgal cell that has rigid cell walls. This excellent interconnection is attributed to the nanostructured surface of the necklace array. The ion-channel-mediated depolarization signature due to a single viral infection was confirmed by delivery of the virus directly to the cell using a scanning probe cantilever. The successful demonstration of noninvasive electrophysiology using a necklace array eFET in this model system has potential application for studying single-cell processes, including entry or exit of medically relevant viruses into or from their host cells. If these processes are related to a viroporin mediated depolarization of the host membrane potential, the kinetics of virus entry and/or exit can be monitored in real time at 10 ms resolution and with high sensitivity. Here, we demonstrated a virus-triggered depolarization of a single cell with an amplitude of *ca.* 40 mV. Judging from the signal-to-noise ratio, the necklace array eFET should hence be sufficiently sensitive to also monitor viroporin induced voltage changes in the hosts of other viruses. For example, the Vpu protein from HIV-1 causes a depolarization in the range of 20–30 mV in mammalian cells,[4] a voltage change which should be well resolved by the necklace array eFET.

To conclude, coupling of an eFET with cantilever-driven viral infection on demand provides a powerful tool for understanding the biophysical processes of entry of some viruses in real time and for screening molecules, which inhibit the early stages of virus infection.

Methods

1. Electrochemical Field-Effect Transistor (eFET) Fabrication.

The preparation of a Au NP necklace solution and the device fabrication procedures were previously described in detail.[17,20] Briefly, a Au NP necklace solution was prepared by adding 50 μL of 20 mM $FeCl_3$ (Sigma-Aldrich, Saint-Louis, MO) into 1 mL of negatively charged 10 nm Au NP (5.7×10^{12} particles/mL, BBI international, Cardiff, U.K.). This reaction results in the colorimetric change of the Au NP solution from red to blue due to conducting electron delocalization (red-shift in the surface plasmon resonance (SPR) band).[19]

Two gold electrodes (230 μm (*W*) × 250 μm (*L*), ~70 μm apart) were prepared by e-beam sputtering through a photoresist mask~10 nm thick Ti adhesion layer on a 500 nm thick thermal oxide-coated silicon wafer with a total thickness of the gold pad of ~50 nm. Two typical electrodes for the device with a gap of 70 μm are shown in Figure 1a (inset 2).

The chip was coated with SU8 photoresist, and a 300 μm channel was exposed around the electrode gap by lithography (Figure 1a, inset 1). A prefabricated (1 mm (*L*) × 210 μm (*W*)) poly(dimethylsiloxane) stripe (PDMS, Sylgard 184), inked with hexane−PDMS solution (25:1, weight ratio), was placed across two gold pads and then cured at 60 °C for 5 min. The PDMS stripe was carefully removed, and the stamped PDMS ink was further baked at 60 °C for 120 min. The device was then treated by NH_3 plasma for 1 min to functionalize the PDMS patterned surface with the positively charged amine groups. The chip was immersed in 350 μL of the Au NP necklace solution for 18 h. The device was carefully washed with deionized (DI) water to remove the unbound Au NP necklace particles and dried with N_2. The array exclusively deposited on the PDMS strip.[20] The necklace array deposited continuously across the SiO_2/Au interface making excellent electrical contact with the electrode (Figure 1a). Both Au pads were hermetically sealed with a polymer film (cyanoacrylate adhesive, LOCTITE, Henkel Corp., Westlake, OH) after Au NP necklace deposition.[13] Thus, only the necklace array located in the gap of the two gold pads was in contact with the electrolyte solution.

2. Electronic Characteristics of Necklace Array in Water.

The eFET was essentially driven by the well-known "four-electrode" arrangement used in electrochemical analysis (Figure S1).[17] The two

working electrodes, the source and the drain, were at a constant bias, V_{SD}, where the source was grounded. The solution was maintained at a potential V_g with respect to the source using a high impedance reference electrode. In our arrangement, the reference electrode was the well-known Ag/AgCl system. The fourth electrode, known as the counter electrode (not shown in the schematic), was a Pt wire dipped in the solution. The eFET was driven by a standard electrochemical instrument called the bipotentiostat where the current V_g was ramped at fixed V_{SD}. The bipotentiostat measured the current I_1 and I_2 between the counter electrode and the source and the drain, respectively. On the basis of previous calculations shown for this eFET arrangement,[13] the device current was $I_{SD} = (I_1 - I_2)/2$.

3. Microalgae Culture and Chlorovirus Purification.

The PBCV-1 host *C. variabilis* was grown on a modified bold basal medium by the addition of 0.5% sucrose and 0.1% peptone (MBBM, pH 7.0)[28] under continuous illumination with shaking at 150 rpm at 25 °C. The Chlorovirus *Paramecium bursaria* chlorella virus (PBCV-1) was grown and purified as described previously.[29] The virus concentration was determined by A^{260} values and by a plaque assay (PFU per mL).[30] The purified virus particles were stored at 4 °C prior to use.

4. Virus Injection into the Device Using a Syringe.

The device was spin-coated with 3 mg·mL^{-1} of PLL (Sigma-Aldrich, Saint-Louis, MO) at 3000 rpm for 30 s. The device was washed with DI water to remove the residues of PLL, and carefully dried with N_2. *Chlorella* cells ((1−2) × 10^7 cells/mL) were deposited on the PLL-coated device for 10 min (Figure 2a). Thus, the microalgae were noninvasively in contact with the Au NP necklace arrays (Figure 2a, insets). The device was placed into a home-built electrochemical chamber (Upilex). A Ag/AgCl reference electrode (RE, 3 M KCl, Warner Instruments, LLC, Hamden, CT) and a Pt wire counter electrode (CE, diameter of ∼10 μm) were inserted into the chamber (Figure 1c). The device was filled with MBBM solution with 0.5 mM $MgCl_2$ as the electrolyte. The MBBM solution consisted of $NaNO_3$ (2.94 mM), $CaCl_2{\cdot}2H_2O$ (0.17 mM), $MgSO_4{\cdot}7H_2O$ (0.3 mM), KH_2PO_4 (1.29 mM), K_2HPO_4 (0.43 mM), NaCl (0.43 mM), H_3BO_3 (0.19 mM), $Na_2{\cdot}$EDTA (0.17 mM), KOH (0.55 mM), and $FeSO_4{\cdot}7H_2O$ (17.9 μM), plus trace elements of $ZnSO_4{\cdot}7H_2O$ (30 μM), $MnCl_2{\cdot}4H_2O$ (7.3 μM),

MoO_3 (4.9 μM), $CuSO_4 \cdot 5H_2O$ (6.3 μM), and $Co(NO_3)_2 \cdot 6H_2O$ (1.7 μM). The needle of a syringe was placed in the electrochemical chamber and located approximately 5 mm from the electrode surface (as schematically shown in Figure S3). One hundred microliters of viral suspension (5×10^8 PFU/mL in 5 mM Tris-HCl buffer with 0.5 mM $MgCl_2$, pH 7.8) was carefully injected onto the microalgae-deposited Au NP necklace arrays (Figure S3). Two Au working electrodes (WE1 and WE2), CE, and RE were connected to a bipotentiostat (PGSTAT 128N, Metrohm Autolab B.V., Utrecht, The Netherlands), and the device was operated at a constant bias of $V_{SD} = -0.5$ V and $V_g = 0$ mV. The resulting current change on the device was concomitantly measured by the bipotentiostat as the virus particles were added into the chamber through a syringe system. As the particles were diffused into the chamber, viral infection of microalgae deposited on the necklace array device occurred leading to a change in the device current I_{SD} (Figure 2b).

5. Virus Particle Injection Using a Scanning Probe Microscope Cantilever System.

The silicon scanning probe microscope cantilever (400 μm (L) × 50 μm (W), AppNano, Mountain View, CA) was glued on the titanium bar (~6 cm (L) × ~0.4 cm (W) × ~0.15 cm (H), Figure 4b) using epoxy to easily manipulate the cantilever inside the electrochemical cell. The cantilever glued titanium bar was treated with O_2 plasma for 1 min and then dipped into 3 mg·mL^{-1} of PLL solution for 2 h. The cantilever was then immersed into the virus solution for 2 h at 4 °C to immobilize the virus particles on the PLL-coated cantilever surface (Figure 4b). The cantilever was carefully washed with 5 mM Tris-HCl, 0.5 mM $MgCl_2$ solution, pH. 7.8, to remove unbound virus particles, followed by washing with DI water. The titanium bar was then installed on the motorized x, y, z-nanomotion stage (PI Piezo Nanopositioner, PI) and inserted into the electrochemical cell. Once the cantilever was positioned above the gap of the two Au pads of the device (the cantilever was out of focus, as shown in Figure 4c, left), the cantilever vertically approached the device using the E-816 computer interface at the rate of 200 nm·min^{-1}. Once the cantilever touched the microalgae-deposited NP necklace array, the cantilever clearly appeared on the CCD camera (Figure 4c, right). Furthermore, the current measured by the eFET immediately decreased as the cantilever landed. The cantilever stayed on top of the microalgae-deposited

necklace arrays after landing which introduced rapid viral infection of the microalgae, and the current change during the viral infection process was concomitantly measured by the bipotentiostat (Figure 4d).

Supporting Information follows the **References**: six subsections and five figures describing a schematic setup to measure electronic characteristics of necklace array in water, biological events associated with viral infection and without viral infection, a model for biogating experiment, real-time membrane potential calculation, and ion concentration and flux calculation.

The authors declare no competing financial interest.

Acknowledgments — Special thanks go to Jim Gurnon for preparing the virus and the microalgal cells. This research was supported by the U.S. Department of Energy, Office of Basic Energy Sciences (DESC0001302) (R.F.S.), the National Research Foundation of Korea (NRF-2014R1A1A3051952) (E.-H.L.), the LOEWE initiative iNAPO (G.T.), NSF-EPSCoR Grant EPS-1004094 (J.L.V.E.), Stanley Medical Research Institute Grant 11R-0001 (J.L.V.E.), and the COBRE program of the National Center for Research Resources Grant P20-RR15535 (J.L.V.E.). R.F.S. and J.L.V.E. acknowledge support from the Office of Research and Economic Development at UNL.

References

(1) Pinto, L. H.; Holsinger, L. J.; Lamb, R. A. Influenza Virus M2 Protein Has Ion Channel Activity. *Cell* 1992, *69*, 517–528.

(2) Nieva, J. L.; Madan, V.; Carrasco, L. Viroporins: Structure and Biological Functions. *Nat. Rev. Microbiol.* 2012, *10*, 563–74.

(3) Thiel, G.; Moroni, A.; Dunigan, D.; Van Etten, J. L. Initial Events Associated with Virus PBCV-1 Infection of *Chlorella* NC64A. *Prog. Bot.* 2010, *71*, 169–183.

(4) Hsu, K.; Han, J.; Shinlapawittayatorn, K.; Deschenes, I.; Marbán, E. Membrane Potential Depolarization as a Triggering Mechanism for Vpu-Mediated HIV-Release. *Biophys. J.* 2010, *99*, 1718–1725.

(5) Boulanger, P.; Lettelier, L. Ion Channels are Likely to be Involved in the Two Steps of Phage T5 DNA Penetration into *Escherichia coli* Cells. *J. Biol. Chem.* 1992, *267*, 3168–3172.

(6) Liang, X.; Li, Z.-Y. Ion Channels as Antivirus Targets. *Virol. Sin.* 2010, *25*, 267–280.

(7) Brauner, T.; Hulser, D. F.; Strasser, R. J. Comparative Measurements of Membrane Potentials with Microelectrodes and Voltage-Sensitive Dyes. *Biochim. Biophys. Acta, Biomembr.* 1984, *771*, 208–216.

(8) Fromherz, P.; Offenhausser, A.; Vetter, T.; Weis, J. A Neuron- Silicon Junction: a Retzius Cell of the Leech on an Insulated-Gate Field- Effect Transistor. *Science* 1991, *252*, 1290–1293.

(9) Wrobel, G.; Seifert, R.; Ingebrandt, S.; Enderlein, J.; Ecken, H.; Baumann, A.; Kaupp, U. B.; Offenhausser, A. Cell-Transistor Coupling: Investigation of Potassium Currents Recorded with p- and n-Channel FETs. *Biophys. J.* 2005, *89*, 3628–3638.

(10) Zeck, G.; Fromherz, P. Noninvasive Neuroelectronic Interfacing with Synaptically Connected Snail Neurons Immobilized on a Semiconductor Chip. *Proc. Natl. Acad. Sci. U. S. A.* 2001, *98*, 10457– 10462.

(11) Lu, W.; Xie, P.; Lieber, C. M. Nanowire Transistor Performance Limits and Applications. *IEEE Trans. Electron Devices* 2008, *55*, 2859– 2876.

(12) Parrish, K. N.; Akinwande, D. Impact of Contact Resistance on the Transconductance and Linearity of Graphene Transistors. *Appl.*

(13) Yu, C.; Lee, S. W.; Ong, J.; Moore, D.; Saraf, R. F. Single Electron Transistor in Aqueous Media. *Adv. Mater.* 2013, *25*, 3079–3084.

(14) Cui, Y.; Wei, Q.; Park, H.; Lieber, C. M. Nanowire Nanosensors for Highly Sensitive and Selective Detection of Biological and Chemical Species. *Science* 2001, *293*, 1289–1292.

(15) Krüger, M.; Buitelaar, M. R.; Nussbaumer, T.; Schönenberger, C.; Forró, L. Electrochemical Carbon Nanotube Field-Effect Transistor. *Appl. Phys. Lett.* 2001, *78*, 1291–1293.

(16) Chen, F.; Qing, Q.; Xia, J.; Li, J.; Tao, N. Electrochemical Gate- Controlled Charge Transport in Graphene in Ionic Liquid and Aqueous Solution. *J. Am. Chem. Soc.* 2009, *131*, 9908–9909.

(17) Lee, E. H.; Lee, S. W.; Saraf, R. F. Noninvasive Measurement of Membrane Potential Modulation in Microorganisms: Photosynthesis in Green Algae. *ACS Nano* 2014, *8*, 780–786.

(18) Kane, J.; Ong, J.; Saraf, R. F. Chemistry, Physics, and Engineering of Electrically Percolating Arrays of Nanoparticles: a Mini Review. *J. Mater. Chem.* 2011, *21*, 16846–16858.

(19) Maheshwari, V.; Kane, J.; Saraf, R. F. Self-Assembly of a Micrometers-Long One-Dimensional Network of Cemented Au Nanoparticles. *Adv. Mater.* 2008, *20*, 284–287.

(20) Ong, J. K.; Nguyen, C. V.; Sayood, S.; Saraf, R. F. Imaging Electroluminescence from Individual Nanoparticles in an Array Exhibiting Room Temperature Single Electron Effect. *ACS Nano* 2013, *7*, 7403–7410.

(21) Van Etten, J. L.; Dunigan, D. D. Chloroviruses: Not Your Everyday Plant Virus. *Trends Plant Sci.* 2012, *17*, 1–8.

(22) Romani, G.; Piotrowski, A.; Hillmer, S.; Gurnon, J.; Van Etten, J. L.; Moroni, A.; Thiel, G.; Hertel, B. A Virus-Encoded Potassium Ion Channel is a Structural Protein in the Chlorovirus *Paramecium bursaria Chlorella* Virus 1 Virion. *J. Gen. Virol.* 2013, *94*, 2549–2556.

(23) Kane, J.; Inan, M.; Saraf, R. F. Self-Assembled Nanoparticle Necklaces Network Showing Single-Electron Switching at Room Temperature and Biogating Current by Living Microorganisms. *ACS Nano* 2010, *4*, 317–323.

(24) Zhou, H. B.; Li, G.; Sun, X. N.; Zhu, Z. H.; Jin, Q. H.; Zhao, J. L.; Ren, Q. S. Integration of Au Nanorods with Flexible Thin-Film Microelectrode Arrays for Improved Neural Interfaces. *J. Microelectromech. Syst.* 2009, *18*, 88–96.

(25) Agarkova, I.; Hertel, B.; Zhang, X.; Lane, L.; Tchourbanov, A.; Dunigan, D. D.; Thiel, G.; Rossmann, M. G.; Van Etten, J. L. Dynamic Attachment of Chlorovirus PBCV-1 to *Chlorella variabilis*. *Virology* 2014, *466–467*, 95–102.

(26) Komor, E.; Tanner, W. Determination of the Membrane Potential of *Chlorella vulgaris*. *Eur. J. Biochem.* 1976, *70*, 197–204.

(27) Pagliuca, C.; Goetze, T. A.; Wagner, R.; Thiel, G.; Moroni, A.; Parcej, D. Molecular Properties of Kcv, a Virus Encoded K^+ Channel. *Biochemistry* 2007, *46*, 1079–1090.

(28) Van Etten, J. L.; Burbank, D. E.; Xia, Y.; Meints, R. H. Growth Cycle of a Virus, PBCV-1, That Infects *Chlorella*-Like Algae. *Virology* 1983, *126*, 117–125.

(29) Agarkova, I. V.; Dunigan, D. D.; Van Etten, J. L. Virion-Associated Restriction Endonucleases of Chloroviruses. *J. Virol.* 2006, *80*, 8114– 8123.

(30) Van Etten, J. L.; Burbank, D. E.; Kuczmarski, D.; Meints, R. H. Virus Infection of Culturable *Chlorella*-Like Algae and Development of a Plaque Assay. *Science* 1983, *219*, 994–996.

Supporting Information follows

Supplemental Information

Noninvasive Measurement of Electrical Events Associated with a Single Chlorovirus Infection of a Microalgal Cell

Seung-Woo Lee,[§, 1, 4] Eun-Hee Lee,[§, 1, 5]

Gerhard Thiel,[2] James L. Van Etten,[3] Ravi F. Saraf [1,6*]

[1]Department of Chemical and Biomolecular Engineering, University of Nebraska-Lincoln, Lincoln, Nebraska 68588, USA; [2]Department of Biology, Technische Universität-Darmstadt, Schnittspahnstrasse 3, 64287, Germany; [3]Department of Plant Pathology and Nebraska Center for Virology, University of Nebraska-Lincoln, Nebraska 68583, USA; [4]Post-Silicon Semiconductor Institute, Korea Institute of Science and Technology (KIST), Hwarang-ro 14-gil 5, Seongbuk-gu, Seoul 02792, Republic of Korea; [5]Department of Environmental Science and Engineering, Ewha Womans University, Ewhayeodae-gil 52, Seodaemun-gu, Seoul 03760, Republic of Korea; [6]Nebraska Center for Materials and Nanosciences, University of Nebraska-Lincoln, Lincoln, Nebraska 68588, USA.

[§] S.-W. Lee and E.-H. Lee contributed equally to this paper.

[*] Corresponding author: Ravi F. Saraf, E-mail address: rsaraf2@unl.edu

[**] This research was supported by the U.S. Department of Energy, Office of Basic Energy Sciences (DE-SC0001302) (RS), the National Research Foundation of Korea (NRF-2014R1A1A3051952) (EHL), the LOEWE initiative iNAPO (GT), NSF-EPSCoR grant EPS-1004094 (VE), Stanley Medical Research Institute Grant 11R-0001 (VE), and the COBRE program of the National Center for Research Resources Grant P20-RR15535 (VE). RS and VE acknowledge support from the Office of Research and Economic Development at UNL.

A. Schematic Set-up to Measure Electronic Characteristics of necklace array in water

The electrochemical field-effect transistor (eFET) was essentially driven by the well known "four-electrode" arrangement used in electrochemical analysis (Fig. S1).[1] The two working electrodes, the source and the drain, were at a constant bias, V_{SD}, where the source was grounded. The solution was maintained at a potential V_g with respect to the source using a high impedance reference electrode. In our arrangement, the reference electrode was the well-known Ag/AgCl system. The fourth electrode, known as the counter electrode (not shown in the schematic) was a Pt wire dipped in the solution. The eFET was driven by a standard electrochemical instrument called the bipotentiostat where the current V_g was ramped at fixed V_{SD}. The bipotentiostat measured the current I_1 and I_2 between the counter electrode and the source and the drain, respectively. Based on previous calculations shown for this eFET arrangement,[2] the device current was $I_{SD} = (I_1 - I_2)/2$.

B. Biological events associated with viral infection

The major steps involved in viral infection of *C. variabilis* by the PBCV-1 virus are outlined in Fig. S2. In the first step, (i) the virus comes into contact with the host cell wall at a unique vertex.[3, 4] After attachment, (ii) the host cell wall is degraded by a hydrolytic enzyme(s) secreted by the virion particle.[3, 5] After attachment and wall digestion, (iii) the virus internal membrane fuses with the host plasma membrane, fusion results in the depolarization of the host plasma membrane,[6] followed by the rapid release of K^+ from the cell.[7, 8] The rapid loss of K^+ and associated water fluxes from the host cell reduce cellular turgor pressure, which probably aids ejection of viral DNA and virion-associated proteins into the cell.[9] Pertinent to this manuscript, the viral internal membrane contains a viral-encoded K^+ channel,[8] which is presumably activated when the viral membrane fuses with the host plasma membrane that leads to the depolarization of the host membrane and the release of host cell osmolytes including K^+ ions.[9]

C. No viral infection

Due to the low probability of virus binding and the small area of the device, virus infection does not always occur. A typical response where no infection was observed is shown in Fig.

S4. The signal for the case of injection (Fig. S4(a)) and cantilever mediated infection (Fig. S4(b)) is nominally unresponsive compared to the corresponding change recorded in Fig. 2(b) and Fig. 4(d), respectively.

D. Model for biogating experiment

For the experiments with cells on the device (Fig. S3), the conduction can be considered *via* two types of percolation network paths connecting the source and drain electrodes: (a) a special set of channels that pass through the cell that will be infected; and (b) the other channels that do not pass through the infected cell. Owing to the one-dimensional nature and reasonably low density of the necklace network, these sets of channels are assumed to be parallel to each other with insignificant overlap. Thus, the percolation paths passing under the infected cell were parallel to the rest of the conduction channels between the source and the drain leading to the simple equivalent circuit (Fig. S5). For each set of channels, part of the necklace was covered by the cell while the rest was exposed to the solution. Assuming the morphology of the two types of channels were similar, the resistance of the two channels scale by x, *i.e.*, (R_C+R_S) and x(R_C+R_S) (Fig. S5). The resistances, R_C and R_S, were equivalent to the necklace network under the cell and exposed to the solution, respectively. Because only a few (parallel) percolation paths were under the infected cell, x > 1 for large cell coverage.

Generally, the model of the device was as follows: The network was covered with the cells and the uncovered area was exposed to the solution. Before infection, at homeostasis, the gating potential V_g for the necklace under the cell and the necklace array exposed to the solution was φ_M and 0, respectively. Thus, their resistivities were different (see Equation (5)). For *Chlorella*, $\varphi_M \approx -125$ mV. The conductance of the cell-covered network was higher than the necklace array exposed to the solution because the latter was at a higher V_g (Fig. 1(d)). On exposure to viral particles, the membrane potential of the infected cell modulated on viral attack leading to a change in V_g by $\Delta\varphi$. To incorporate this effect, an additional resistance R_g was added to the part of the network under the cell that modulates by ΔR_g on infection.

The current I_{SD} is the total current that flows through the three parallel necklace networks (Fig. S5). Based on the equivalent diagram (Fig. S5) for an applied external potential, V_{SD}

$$I_g = \left[\frac{1}{(xR_C+xR_S+R_g)}\right] V_{SD} \qquad (1)$$

Due to the viral infection, R_g changes are a small amount, ΔR_g, leading to modulation in the device current $\Delta I_{SD} = \Delta I_g$ given by Equation (1), as

$$\Delta I_g = \left[-\frac{\Delta R_g}{(xR_C+xR_S+R_g)^2}\right] V_{SD} = \Delta I_{SD} \quad (2)$$

From Ohm's law, $V_{SD} = I_g(xR_C+xR_S)+I_gR_g$. Thus, $I_g\Delta R_g = -[xR_C+xR_S-R_g]\Delta I_g$. Furthermore, we assume that rQCD was uniform over the network, *i.e.*, constant transconductance. By definition, $\Delta I_g = g_m\Delta\varphi$. Thus,

$$\Delta R_g = -\frac{(xR_C+xR_S)}{I_g} g_m \Delta\varphi \quad (3)$$

Substituting I_g from Equation (1) into Equation (3) and then substituting the resulting ΔR_g in Equation (2) yielded

$$\Delta\varphi = -\left[\frac{R_g}{xR_C}\left(1+\frac{xR_S}{xR_C}\right)^{-1}+1\right]\frac{1}{g_m}\Delta I_{SD} = -k\frac{1}{g_m}\Delta I_{SD} \quad (4)$$

Next, we estimated the parameter k in Equation (4).

As the thickness and length of the two networks were nominally similar, the only geometrical difference was the effective width. The larger the area coverage, the larger the effective width and, hence, the lower the resistance. Thus, $(xR_C/xR_S) = (R_C/R_S) \sim (A_S/A_C)$, where A_S and A_C are area coverage of the network exposed to the solution and cell, respectively. Furthermore, the g_m for the necklace network exposed to the cell and the solution, $g_{m,c}$ and $g_{m,s}$, respectively, were not the same because they were at V_g of φ_M and 0, respectively. Assuming f is the fraction of the device area covered by the cells, the resulting resistance ratio was

$$\frac{R_C}{R_S} = \frac{xR_C}{xR_S} = \left(\frac{g_{m,S}}{g_{m,C}}\right)\left(\frac{A_S}{A_C}\right) = \left(\frac{g_{m,S}}{g_{m,C}}\right)\frac{f}{1-f} \quad (5)$$

We note that $(xR_C/xR_S) = (R_C/R_S)$ assumes that the network morphology was reasonably uniform at 10 μm scale (the size of a cell).

To estimate xR_C/R_g, we assumed that the percolation path that passed through the infected cell was nominally the length (L) of the array (*i.e.*, 70 μm). Thus, the length of the array under the cell was fL. Similarly, the length of the array under the infected cell was about 10 μm. Thus,

$$\frac{xR_C}{R_g} = \frac{fL-10}{10} = 7f-1 \quad (6)$$

Due to the low density network of one dimensional necklaces, the assumption in Equation (6) was reasonable.

Substituting Equations (5) and (6) in Equation (4) where $g_m = g_{m,C}$,

$$\Delta\varphi = \varphi - \varphi_M = -\left[\frac{1}{(7f-1)}\left(1+\left\{\frac{g_{m,S}}{g_{m,C}}\right\}\frac{f}{1-f}\right)^{-1}+1\right]\frac{1}{g_{m,C}}\Delta I_{SD} = -k\frac{1}{g_{m,C}}\Delta I_{SD} \quad (7)$$

where φ is the membrane potential at some time t after the infection.

E. Calculation of the real-time membrane potential

The change in membrane potential $\Delta\varphi(t)$ was quantified by considering the device's operating condition. The necklace network exposed to the medium and the cells was at $V_g = 0$ mV and $V_g = \varphi_M$, where φ_M was the resting membrane potential of the cell, respectively. For *Chlorella*, $\varphi_M \approx -125$ mV,[10] thus, from transconductance (Fig. 1(d)), $g_{m,S}$ and $g_{m,C}$ are 6 nS and 8nS, respectively. For the device, typically, f = 0.25 (Fig. 2(a)).

Before the infection, $I_{SD} \sim$ -2.4 nA leading to $\Delta I_{SD} = I_{SD}$ - (-2.4 nA). Substituting the above mentioned constants (f, $g_{m,S}$ and $g_{m,C}$) in Equation (7), $\varphi(t)$ was obtained. Setting $\Delta\varphi = \varphi(t) - \varphi(0)$, $\Delta\varphi(t)$ was calculated (see Fig. 2(c)).

F. Calculation of ion concentration and flux

Due to difference in K^+ concentration, let φ and φ_s be the potential inside the cell and in the solution, respectively. The reference potential was defined by setting $\varphi_s = 0$. Let the concentration of K^+ ions inside and media be $[K^+]$ and $[K^+]_s$, respectively. Thus, the membrane potential due to K^+ ion from the Nernst's equation wass given by

$$\varphi - \varphi_s = -59.5log\left(\frac{[K^+]}{[K^+]_s}\right)mV \quad (8)$$

The potentials are in mV.

At t = 0, just before the infection, $\varphi = \varphi_M$ the resting potential. Substituting the initial condition in Equation (8),

$$\Delta\varphi = \varphi - \varphi_M = -59.5log\left(\frac{[K^+]}{[K^+]_M}\right)mV \quad (9)$$

where, $[K^+]_M$ was the concentration of K^+ in the homeostatic state.

Typically, for *Chlorella*, $[K^+]_M \sim 100$ mM.[11]

Assume the average diameter of the cell was 5 μm and the fraction of cytoplasm was 30%. But the other 70% contained an aqueous solution with K^+ which was flux continuum with the cytosol. When K^+ is lost from the cytosol, it will be refilled for some time from the interior compartments. Thus, the number of K^+ ions in the cell, N, leading to membrane potential modulation was nominally all of the cell volume leading to

$$N \approx 3.93x10^7[K^+] \quad (10)$$

From $\Delta I_{SD}(t)$ response in Figs. 2(b), $\Delta\varphi(t)$ is calculated by Equations (7) and substituted in Equation (9) to compute $[K^+]$ as a function of time, t. Substituting, $[K^+](t)$ in Equation (10) and taking the derivative of both sides, dN/dt was computed. Fig. 1(c) show the ion flux dN/dt and $\Delta\varphi(t)$ as a function of t.

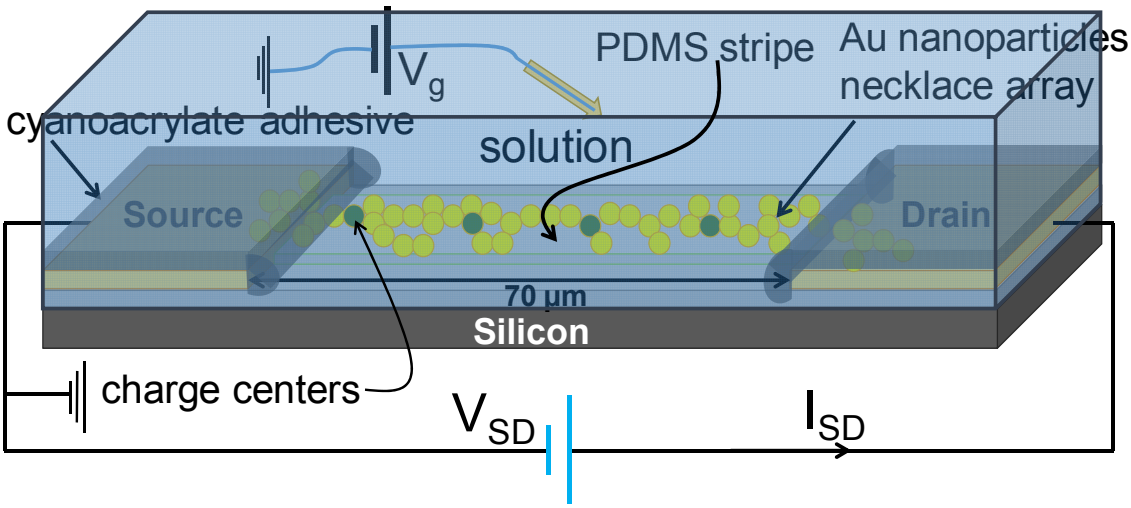

Fig. S1. Schematic of experimental setup for the electrochemical gating assay using a bipotentiostat.

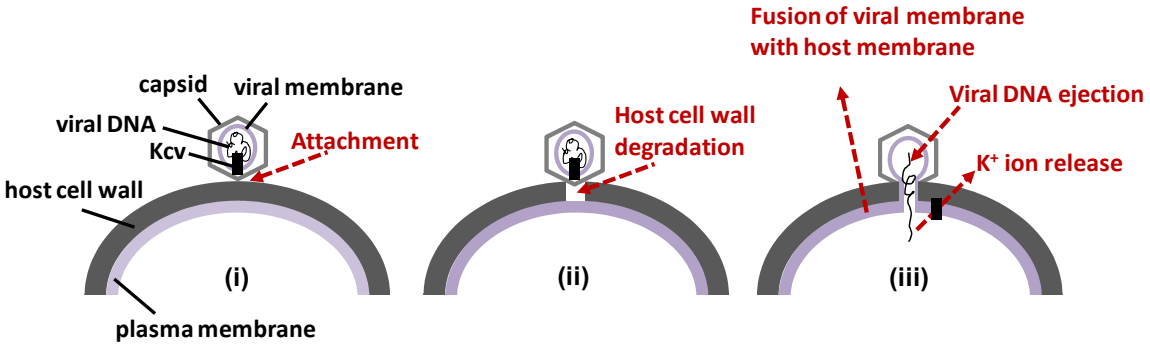

Fig. S2. Schematic of the early viral infection processes on algae.

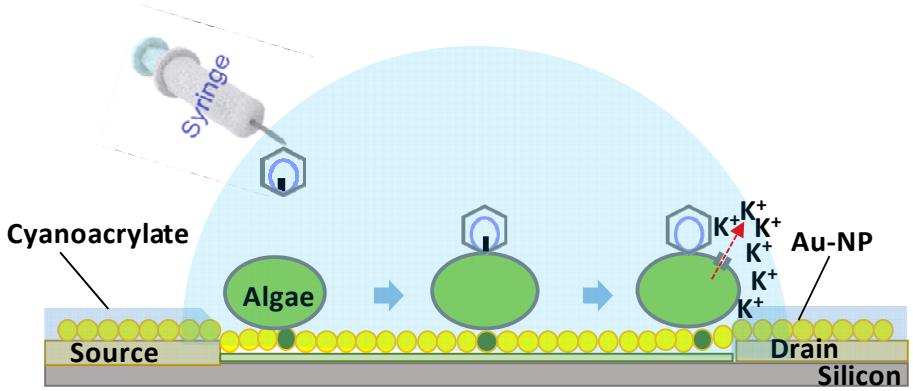

Fig. S3. Biogating response caused by the viral infection of algae which were deposited on the Au NP necklace arrays. Schematic of the overall viral infection processes on algae-deposited eFET device which were introduced *via* a syringe injection system.

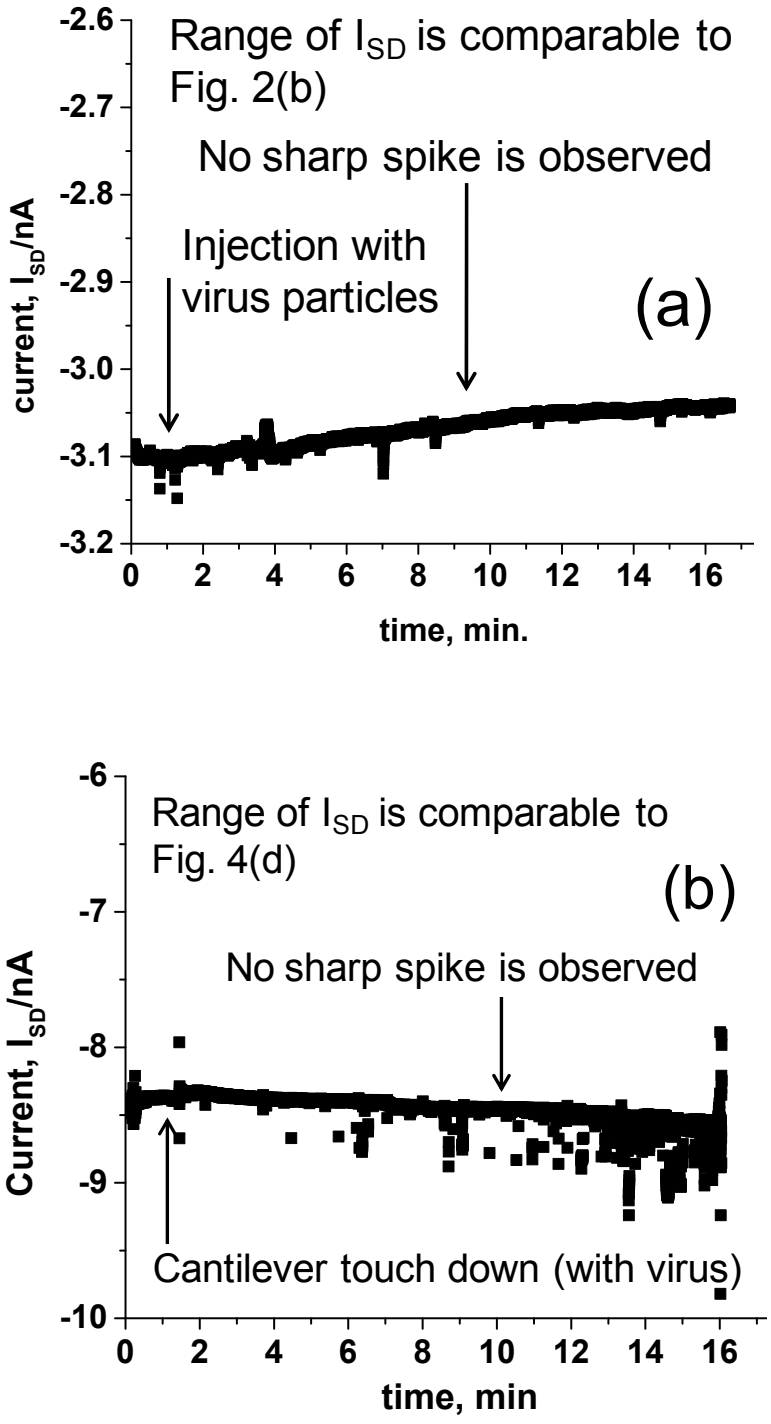

Fig. S4. Response of necklace array eFET where no virus infection occurred. (a) Injection of virus similar to Fig. 2(b). (b) Cantilever mediated virus delivery similar to Fig. 4(d).

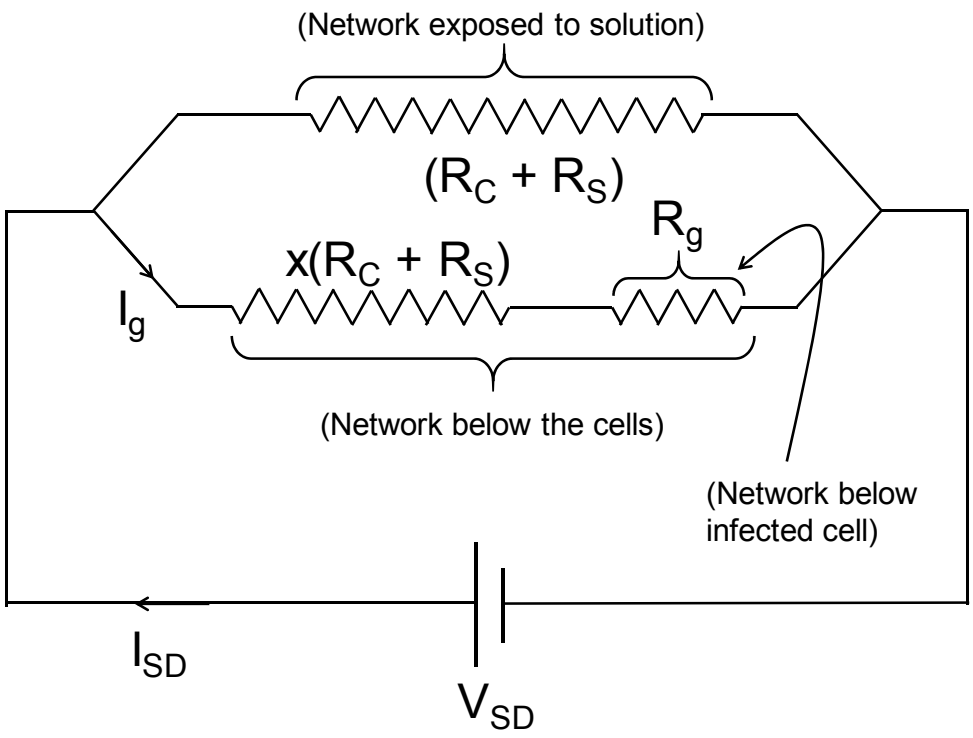

Fig. S5. Schematic diagram of the necklace network under the cells and exposed to the solution. V_{SD} and I_{SD} are an applied voltage and the measured current between the source and drain electrodes, respectively. I_g is the current through the network below the cell. Rs, Rc, and Rg indicate the network effective resistances of the solution, cells exposed to the network, and cells infected by the virus, respectively.

References

(1) Lee, E. H.; Lee, S. W.; Saraf, R. F. Noninvasive Measurement of Membrane Potential Modulation in Microorganisms: Photosynthesis in Green Algae. *ACS Nano* **2014**, 8, 780-786.

(2) Yu, C.; Lee, S. W.; Ong, J.; Moore, D.; Saraf, R. F. Single Electron Transistor in Aqueous Media. *Adv. Mater.* **2013**, 25, 3079-3084.

(3) Meints, R. H.; Lee, K.; Burbank, D. E.; Van Etten, J. L. Infection of a *Chlorella*-like Alga with the Virus, PBCV-1: Ultrastructural Studies. *Virology* **1984**, 138, 341-346.

(4) Zhang, X.; Xiang, Y.; Dunigan, D. D.; Klose, T.; Chipman, P. R.; Van Etten, J. L.; Rossmann, M. G. Three-Dimensional Structure and Function of the *Paramecium bursaria* Chlorella Virus Capsid. *Proc. Natl. Acad. Sci. USA* **2011**, 108, 14837-14842.

(5) Van Etten, J. L.; Dunigan, D. D. Chloroviruses: not Your Everyday Plant Virus. *Trends Plant Sci.* **2012**, 17, 1-8.

(6) Frohns, F.; Kasmann, A.; Kramer, D.; Schafer, B.; Mehmel, M.; Kang, M.; Van Etten, J. L.; Gazzarrini, S.; Moroni, A.; Thiel, G. Potassium Ion Channels of Chlorella Viruses Cause Rapid Depolarization of Host Cells During Infection. *J. Virol.* **2006**, 80, 2437-2444.

(7) Neupartl, M.; Meyer, C.; Woll, I.; Frohns, F.; Kang, M.; Van Etten, J. L.; Kramer, D.; Hertel, B.; Moroni, A.; Thiel, G. Chlorella Viruses Evoke a Rapid Release of K^+ from Host Cells During the Early Phase of Infection. *Virology* **2008**, 372, 340-348.

(8) Romani, G.; Piotrowski, A.; Hillmer, S.; Gurnon, J.; Van Etten, J. L.; Moroni, A.; Thiel, G.; Hertel, B. A Virus-Encoded Potassium Ion Channel is a Structural Protein in the *Chlorovirus Paramecium bursaria* Chlorella Virus 1 Virion. *J. Gen. Virol.* **2013**, 94, 2549-2556.

(9) Thiel, G.; Moroni, A.; Dunigan, D.; Van Etten, J. L. Initial Events Associated with Virus PBCV-1 Infection of *Chlorella* NC64A. *Prog. Bot.* **2010**, 71, 169-183.

(10) Komor, E.; Tanner, W. Determination of the Membrane Potential of *Chlorella vulgaris*. *Eur. J. Biochem.* **1976**, 70, 197-204.

(11) Beilby, M. J.; Blatt, M. R. Simultaneous Measurements of Cytoplasmic K Concentration and the Plasma Membrane Electrical Parameters in Single Membrane Samples of *Chara corallina*. *Plant Physiol.* **1986**, 82, 417-422.